

Nanoscale interaction layer at the interface between Al films and SiO₂ substrates of Al/AIO_x/Al Josephson tunnel junctions

L. J. Zeng,¹ T. Greibe,² S. Nik,¹ C. M. Wilson,² P. Delsing,² and E. Olsson¹

¹*Department of Applied Physics, Chalmers University of Technology, 412 96 Gothenburg, Sweden*

²*Department of Microtechnology and Nanoscience, Chalmers University of Technology, 412 96 Gothenburg, Sweden*

(Received 7 February 2013; accepted 28 March 2013; published online 12 April 2013)

An interaction layer is found at the Al/SiO₂ interface in Al/AIO_x/Al tunnel junctions grown on SiO₂ substrates. The amorphous intermixing layer has an average thickness of about 5 nm. We present the detailed structure of this interfacial layer as determined by transmission electron microscopy. The layer contains alumina with aluminum being octahedrally coordinated according to electron energy loss spectroscopy analysis rather than tetrahedrally coordinated, where the latter coordination is the most common type in amorphous alumina. Depth profiles of the Al-O and Si-O bonding characteristics were also investigated using energy loss near edge structure.

© 2013 AIP Publishing LLC [<http://dx.doi.org/10.1063/1.4801798>]

I. INTRODUCTION

To achieve long coherence time in superconducting quantum electronics, noise in quantum circuits needs to be minimized since it can cause dissipation and destroy the coherence state in the circuits. In recent years, significant research effort is concerned with the origin of the noise and consequently the way to diminish it in the superconducting devices.^{1–6} The charge noise in single electron transistors (SETs) made from Josephson junctions is understood to originate from the dielectric environment of the junctions.^{7,8} Decoherence in superconducting qubits may also be caused by noise originating from defects accommodated at the qubit/dielectric interfaces.^{4,5} Hence, studying the microstructure at the interface between the Josephson junction and the dielectric substrate is of great importance for figuring out the possible sources of noise in Josephson junction based superconducting devices. Though electric measurements on different superconducting devices have provided crucial information about the interaction between the junction and the substrate dielectrics,^{1–8} direct analysis of the interface structure in such junctions is still lacking and is needed for identifying the structural origins of noise.

In this work, we have studied the detailed interface structure between Al/AIO_x/Al tunnel junctions and amorphous SiO₂ substrates by using atomic resolution transmission electron microscopy (TEM). An interaction layer was found at the interface by both TEM and scanning transmission electron microscopy (STEM) imaging. The elemental distribution and local chemical state of the material at the interface were analyzed using energy filtered transmission electron microscopy (EFTEM) and electron energy loss spectroscopy (EELS). The high spatial resolution of our STEM and EELS data, which reaches beyond 1 nm, also reveals further details about the change in atomic structure as a function of distance from the film/substrate interface compared to previous studies on the reaction at Al/SiO₂ interface under different circumstances.^{9–19} In addition, we found a novel form of alumina in the interaction layer

according to TEM analysis. The interaction at the interface and the special structure of the material in the interaction layer may provide new insights about the effect of the dielectric environment on the junctions in these superconducting devices.

II. EXPERIMENT

The Al/AIO_x/Al tunnel junctions were deposited on SiO₂ (0.4 μm)/Si (350 μm) substrates. The bottom Al electrode layer was thermally deposited with a rate of about 10 Å/s with the substrate at room temperature. The Al layer was then exposed to 0.1 millibar of oxygen during 10 min resulting in a thin AIO_x film on the surface of the Al layer. The top Al electrode was deposited in the same way as the bottom Al layer but with longer deposition time to form a thicker top layer. The nominal thicknesses of the Al layers were 15 nm and 60 nm, respectively. The tunnel junctions with a junction area of 0.08 μm² (400 nm width and 200 nm overlap length) had a normal resistance of ~1 kΩ and low subgap current.²⁰ Both patterned and unpatterned samples were used in our study.

Cross-section TEM samples were prepared by mechanical polishing and dimpling followed by argon ion milling to electron transparency. A Philips CM200 TEM with a field emission gun and equipped with a Gatan Imaging Filter (GIF) 2000 was used at 200 KV for bright field (BF) TEM imaging and EFTEM. An FEI Titan 80–300 TEM/Scanning TEM (STEM) with probe C_s-corrector and a high energy resolution Tridium GIF was used for STEM imaging and STEM-EELS measurements using 300 kV as accelerating voltage. Annular dark field (ADF) STEM images were acquired using a 19.7 mrad beam convergence angle and ~40–200 mrad detector collection angle. The collection angle for EELS experiments was ~24 mrad. The probe size for the STEM imaging and the STEM-EELS measurements was estimated to be ~1.3 Å by measuring lattice fringes of Au nanoparticles in ADF imaging mode. The energy resolution for the STEM-EELS experiments was about 0.6 eV

measured as the full width at half maximum (FWHM) of the zero-loss peak acquired without the specimen. The DigitalMicrograph and EL/P software were used for EELS and EFTEM data processing.

III. RESULTS AND DISCUSSION

A typical Al/AIO_x/Al tunnel junction on a SiO₂/Si substrate is shown in Fig. 1. Both patterned and unpatterned samples show the same interface structure at the Al/SiO₂ interface. Fig. 1(a) shows an overview of the multilayer structure of the junction. The Al layers are polycrystalline as evidenced by the contrast variation between different crystal grains. In Fig. 1(b), contrast variation appears in the image beneath the bottom Al layer at the Al/SiO₂ interface. The Al layer is crystalline and lattice fringes from the Al grains are clearly visible. The layers beneath the Al are amorphous as evident from diffuse rings in the electron diffraction patterns and the absence of diffraction contrast in the images.

The interfacial region has a lower intensity level compared to the SiO₂. The width of the darker region varies between 4 and 7 nm along the interface (as also can be seen in Fig. 2(a)) and the average width is about 5 nm. The difference in contrast between the interfacial region and the SiO₂ substrate suggests that the mass-thickness is higher of the interfacial region compared to the SiO₂ giving rise to the lower image intensity. A higher mass-thickness of the interfacial region is consistent with the complementary results from ADF STEM imaging, Fig. 1(c), where the intensity level of the interfacial layer now is higher. The ADF intensity at high scattering angles is a result of Rutherford scattering and varies approximately as $Z^{1.7}$ (Z is atomic number).²¹ It is unlikely that the intensity variation is due to a specimen thickness variation since there are no other indications of a step-like thickness variation according to our EFTEM and EELS thickness measurement.

The composition and structure of the interfacial layer were studied using EFTEM and EELS measurements. Fig. 2 shows an EFTEM oxygen map and the corresponding bright

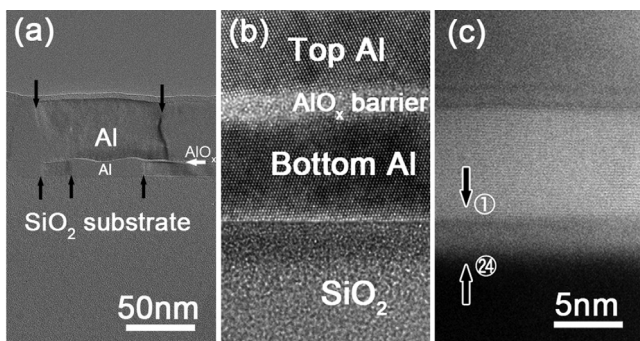


FIG. 1. BF TEM images (a) and (b) and an ADF STEM image (c) of the Al/AIO_x/Al junction grown on SiO₂/Si substrate. The black arrows in (a) indicate the positions of the grain boundaries in the polycrystalline Al films. The contrast variation at the Al/SiO₂ interface is visible in both (b) and (c). The arrows in (c) show the start and end points of the line along which the STEM-EELS spectra were acquired. Numbers 1 and 24 in (c) correspond to the numbers labeled in Fig. 3(a) and indicate the positions where the first and last EELS spectra were acquired in the line scan. The scale bar in (c) also applies to (b).

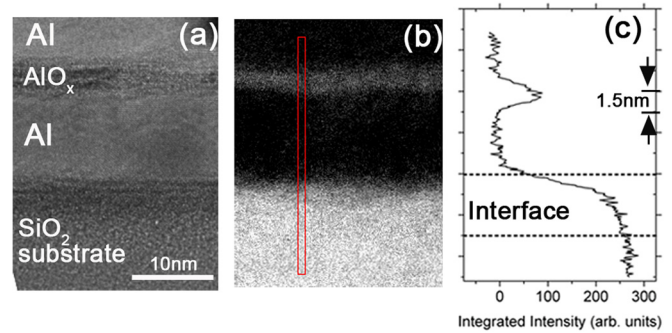


FIG. 2. (a) BF TEM image showing the junction and the substrate. (b) An EFTEM image showing the oxygen map obtained from area (a). (c) The intensity profile from the oxygen map across the interfaces (integrated over the area with a width of about 1.3 nm as indicated in (b)).

field TEM image. A variation of the oxygen signal is observed both at the tunnel barrier and at the Al/SiO₂ interface. The width of the barrier layer (full width at half maximum) is about 1.5 nm and the width of the interfacial layer is about 5 nm.

In order to clarify the composition and structure of the interfacial layer, spatially resolved STEM-EELS analyses were carried out across the interface from the bottom Al layer into the SiO₂ substrate, as shown in Fig. 3(a). The positions where the STEM-EELS spectra were recorded at the interface are marked in Fig. 1(c). Two arrows indicate the start and end positions of the line scan. The background of each EEL spectrum was subtracted using the power-law model.²² The distance between each spectrum was about

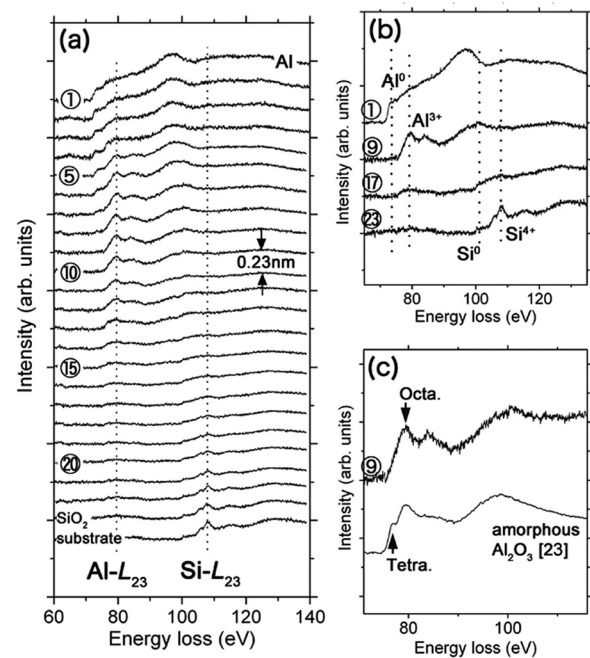


FIG. 3. STEM-EELS spectra taken across the Al/SiO₂ interface. (a) The distance between the positions where the spectra were acquired is about 0.23 nm. The positions of the Al L edge and Si L edge are indicated by dashed lines for clarity. (b) Enlarged spectra 1, 9, 17, and 23 from (a) showing the characteristic L edges of Al⁰ (metallic Al), Al³⁺ (alumina), Si⁰ (elemental Si), and Si⁴⁺ (SiO₂), respectively. (c) Al L₂₃ ELNES obtained at the Al/SiO₂ interface and that of amorphous Al₂O₃.²³ The arrows indicate the peaks corresponding to octahedrally and tetrahedrally coordinated Al sites.

0.23 nm. The Al L_{23} and Si L_{23} energy loss near edge structure (ELNES) changed with position. EEL spectra corresponding to metallic Al (Al^0) (Ref. 23) were obtained in the Al layer, shown as the first spectrum in Figs. 3(a) and 3(b). The midpoint of the edge onset of Al^0 L edge is at 72.5 eV. As the probe moved towards the SiO_2 substrate, the L edge of the metallic Al degraded gradually, while a new edge appeared at about 79.5 eV, followed by a small bump peaked at around 84 eV (spectrum 9 in Figs. 3(a)–3(c)). These features belong to the Al L_{23} edge of alumina (Al^{3+}). Thus, we conclude that alumina is formed at Al/ SiO_2 interface. The shift of the peak at round 97 eV of Al^0 L edge towards the higher energy direction is also visible in Figs. 3(a) and 3(b). Since the L edge of Si^0 arises at around 100 eV and overlaps with Al^0 L edge, this shift indicates the presence of elemental Si (Si^0) in the interfacial layer. As the electron probe moved further towards the SiO_2 , the L edge of Si^0 became more profound while the L edge of Al^{3+} gradually diminished and almost disappeared (spectrum 10 to spectrum 23 in Fig. 3(a)). At the same time, the Si L_{23} edge of SiO_2 started to appear at 105 eV (midpoint of edge onset). The Si^{4+} L_{23} ELNES peak intensity increased gradually towards SiO_2 although the Si^{4+} L_{23} fine structure did not differ in this area (spectrum 20 to 24). The bottom spectrum in Fig. 3(a) is identical to those observed in amorphous SiO_2 and silicates containing SiO_4 tetrahedra.^{24,25}

The free energy of the Al-O bond is lower than that of Si-O, thus the formation of alumina can be understood in terms of breaking the Si-O bonds promoted by impinging Al atoms and clusters during the film deposition combined with formation of the thermodynamically favorable Al and O bonds. The solid-state reaction at the Al/ SiO_2 interface in these Al/ AlO_x /Al Josephson junctions is consistent with previous investigations performed at the interface between Al thin films and SiO_2 prepared at various conditions.^{9–19} This reaction can be described by $4Al + 3SiO_2 = 2Al_2O_3 + 3Si + 176.4 \text{ kcal/mol}$.^{10,12,16,18}

However, there are two points to notice based on our STEM-EELS analysis. First, we found an unusual form of alumina at the Al/ SiO_2 interface resulting from a solid-state reaction. By utilizing techniques such as X-ray photoelectron spectroscopy (XPS) and Auger electron spectroscopy (AES), previous investigations revealed that the interfacial alumina maintains the characteristic of stoichiometric Al_2O_3 .^{10,11} In Ref. 12, the interfacial alumina is identified as η - Al_2O_3 by electron diffraction. We found that the reaction layer at Al/ SiO_2 interface in our junctions is amorphous but the EELS fine structure of the Al L edge (e.g., spectrum 9) of this interfacial layer is different from that of the ordinary amorphous alumina (amorphous- Al_2O_3). The Al L_{23} ELNES acquired in the interfacial layer (spectrum 9) and that of the amorphous Al_2O_3 (adopted from Ref. 23) are both plotted in Fig. 3(c) for comparison. It is known that Al L_{23} ELNES in EELS is sensitive to the coordination of Al in the systems containing Al-O bonding such as alumina and silicate.^{26–29} As confirmed in previous experimental and theoretical studies,^{26–28} the peak at about 79.5 eV arises from the octahedrally coordinated Al cations, while the one near the edge onset at about 77.6 eV is highly characteristic of Al sites

with coordination number four in the amorphous phase.²³ The spectra we obtained from the interfacial region show a profound peak positioned at 79.5 eV and an abrupt edge onset without any fine features in the range from the edge onset to the peak position (Fig. 3(c)). We thus conclude that the amorphous alumina that formed at the Al/ SiO_2 interface has Al and O atoms arranged as AlO_6 octahedra, which resembles the atomic arrangement in crystalline α - Al_2O_3 .

Second, STEM-EELS unveiled the depth distribution of elements with higher spatial resolution compared to other techniques like XPS and AES. In the region close to Al film, Al_2O_3 and Si coexist as a result of the reaction between Al and SiO_2 (spectrum 9 in Figs. 3(a) and 3(b)). In the region further away from Al, the amount of Al_2O_3 decreases and SiO_2 starts to appear while there is still some amount of elemental Si (spectrum 17 in Figs. 3(a) and 3(b)). Even in the region where SiO_2 is dominant in the material, there is still Si coexisting with SiO_2 (e.g., spectrum 23 in Figs. 3(a) and 3(b)). Therefore, our results do not support the ordering model Al/ Al_2O_3 /Si/ SiO_2 in the reacted region^{11,16,17,19} but instead a more diffuse intermixing model as suggested in Refs. 10 and 15. More detailed investigation needs to be carried out in order to clarify the status of atomic distribution at the interface, especially the area between alumina and SiO_2 . In this region, neither Al^{3+} , Si^0 nor Si^{4+} ELNES is obvious in our primary EELS results (e.g., spectrum 17 in Figs. 3(a) and 3(b)), indicating more disordered arrangements among Al, Si, and O. However, the gradual change of the Si^{4+} L_{23} peak intensities in EEL spectra, the coexistence of elemental Si with SiO_2 , as well as the formation of Al-O bonds at the Al/ SiO_2 interface suggest that the migration of O atoms from SiO_2 towards the Al side is likely.

IV. CONCLUSION

In conclusion, we found an amorphous intermixing layer at the interface between the bottom Al layer and the SiO_2 substrate in Al/ AlO_x /Al junctions grown on the SiO_2 /Si substrate using TEM. The intermixing layer is about 5 nm in thickness and consists of alumina in which Al is predominantly octahedrally coordinated. According to the Al ELNES analysis, the Al-O bonding characteristic of the interface alumina layer is different from that of the most common type of amorphous Al_2O_3 in which the Al atoms are predominantly tetrahedrally coordinated. There is a diffused depth distribution of alumina, Si, and SiO_2 at the interface. An intermediate layer was found between the interfacial alumina layer and the SiO_2 , where there is little Al or Si ELNES signal. These results show that there is a redistribution of Al, O, and Si atoms at the junction/substrate interface, which may play an important role in understanding the low frequency charge noise behavior of single electron transistors and decoherence in aluminum based qubits.

ACKNOWLEDGMENTS

We thank the Swedish Foundation for Strategic Research, the Swedish Research Council, and the Knut and Alice Wallenberg Foundation for financial support.

- ¹H. Wang, M. Hofheinz, J. Wenner, M. Ansmann, R. C. Bialczak, M. Lenander, E. Lucero, M. Neeley, A. D. O'Connell, D. Sank, M. Weides, A. N. Cleland, and J. M. Martinis, *Appl. Phys. Lett.* **95**, 233508 (2009).
- ²K. W. Murch, S. J. Weber, E. M. Levenson-Falk, R. Vijay, and I. Siddiqi, *Appl. Phys. Lett.* **100**, 142601 (2012).
- ³R. Barends, J. Wenner, M. Lenander, Y. Chen, R. C. Bialczak, J. Kelly, E. Lucero, P. O'Malley, M. Mariantoni, D. Sank, H. Wang, T. C. White, Y. Yin, J. Zhao, A. N. Cleland, J. M. Martinis, and J. J. A. Baselmans, *Appl. Phys. Lett.* **99**, 113507 (2011).
- ⁴O. Astafiev, Yu. A. Pashkin, Y. Nakamura, T. Yamamoto, and J. S. Tsai, *Phys. Rev. Lett.* **93**, 267007 (2004).
- ⁵J. M. Martinis, K. B. Cooper, R. McDermott, M. Steffen, M. Ansmann, K. D. Osborn, K. Cicak, S. Oh, D. P. Pappas, R. W. Simmonds, and C. C. Yu, *Phys. Rev. Lett.* **95**, 210503 (2005).
- ⁶Z. Kim, B. Suri, V. Zaretsky, S. Novikov, K. D. Osborn, A. Mizel, F. C. Wellstood, and B. S. Palmer, *Phys. Rev. Lett.* **106**, 120501 (2011).
- ⁷G. Zimmerli, T. M. Eiles, R. L. Kautz, and J. M. Martinis, *Appl. Phys. Lett.* **61**, 237 (1992).
- ⁸E. Paladino, L. Faoro, G. Falci, and R. Fazio, *Phys. Rev. Lett.* **88**, 228304 (2002).
- ⁹R. Black, in *Proceedings of the 15th IEEE International Reliability Physics Symposium* (IEEE, New York, 1977), p. 257.
- ¹⁰Y. E. Strausser, E. J. Scheibner, and J. S. Johannesen, *Thin Solid Films* **52**, 203 (1978).
- ¹¹R. S. Bauer, R. Z. Bachrach, and L. J. Brillson, *Appl. Phys. Lett.* **37**, 1006 (1980).
- ¹²S. Roberts and P. J. Dobson, *J. Phys. D: Appl. Phys.* **14**, L17 (1981).
- ¹³J. Derrien, M. Commandre, J. M. Layet, F. Salvan, and A. Cros, *Appl. Phys. A* **28**, 247 (1982).
- ¹⁴R. J. Blattner and A. J. Braundmeier, *J. Vac. Sci. Technol.* **20**, 320 (1982).
- ¹⁵T. Jung and W. Titel, *Phys. Status Solidi A* **74**, 85 (1982).
- ¹⁶M. H. Hecht, R. P. Vasquez, F. J. Grunthaler, N. Zamani, and J. Maserjian, *J. Appl. Phys.* **57**, 5256 (1985).
- ¹⁷Y. Miura and K. Hirose, *J. Appl. Phys.* **79**, 559 (1996).
- ¹⁸F. Dadabhai, F. Gaspari, S. Zukotynski, and C. Bland, *J. Appl. Phys.* **80**, 6505 (1996).
- ¹⁹Y. Miura and K. Hirose, *J. Appl. Phys.* **77**, 3554 (1995).
- ²⁰T. Greibe, M. P. V. Stenberg, C. M. Wilson, T. Bauch, V. S. Shumeiko, and P. Delsing, *Phys. Rev. Lett.* **106**, 097001 (2011).
- ²¹E. J. Kirkland and M. G. Thomas, *Ultramicroscopy* **62**, 79 (1996).
- ²²R. F. Egerton, *Electron Energy-Loss Spectroscopy in the Electron Microscope*, 2nd ed. (Plenum/Springer, New York, 1996), p. 270.
- ²³D. Bouchet and C. Colliex, *Ultramicroscopy* **96**, 139 (2003).
- ²⁴D. A. Muller and G. D. Wilk, *Appl. Phys. Lett.* **79**, 4195 (2001).
- ²⁵K. Kimoto, K. Kobayashi, T. Aoyama, and Y. Mitsui, *Micron* **30**, 121 (1999).
- ²⁶K. Kimoto, Y. Matsui, T. Nabatame, T. Yasuda, T. Mizoguchi, I. Tanaka, and A. Toriumi, *Appl. Phys. Lett.* **83**, 4306 (2003).
- ²⁷R. Brydson, H. Sauer, W. Engel, J. M. Thomas, and E. Zeitler, *J. Chem. Soc., Chem. Commun.* **0**, 1010 (1989); R. Brydson, *J. Phys. D: Appl. Phys.* **29**, 1699 (1996).
- ²⁸P. L. Hansen, R. Brydson, D. W. McComb, and I. Richardson, *Microsc. Microanal. Microstruct.* **5**, 173 (1994).
- ²⁹L. A. J. Garvie and P. R. Buseck, *Am. Mineral.* **84**, 946 (1999).